Mid-infrared dual-comb spectroscopy with room-temperature bi-functional interband cascade lasers and detectors

L. A. Sterczewski,[1] M. Bagheri,[1, a)] C. Frez,[1] C. L. Canedy,[2] I. Vurgaftman,[2] and J. R. Meyer[2]
[1)] *Jet Propulsion Laboratory, California Institute of Technology, Pasadena CA 91109, USA*
[2)] *Naval Research Laboratory, Washington, DC 20375, USA*

Interband cascade (IC) laser structures offer the attractive potential for operating at room temperature as both broadband coherent sources of mid-infrared light and also fast photodetectors. This makes the realization of extremely compact spectrometers on a monolithic platform possible, and even dual-comb spectroscopy (DCS) configurations. IC comb devices are perfect candidates for this configuration, since they develop near-THz-wide optical frequency comb spectra from a millimeter-sized cavity, using a multi-stage structure that can also function as a very fast photodetector. In this work, we leverage IC photodetectors with gigahertz bandwidth to demonstrate a self-contained, free-running, room-temperature DCS system in the mid-infrared. The DCS system used detection by the same bi-functional IC device structure to measure 1,1-difluoroethane over ~600 GHz of optical coverage around 3.6 μm. These results show that the IC platform is suitable for full integration as a broadband, high-resolution on-chip spectrometer in a future chemical sensing system.

The quest for fully-integrated broadband spectrometers has triggered substantial advances in chip-scale light sources, detectors and interferometers. The demand is strong because optical spectroscopy lies at the core of numerous fields ranging from remote sensing[1], medical[2], and pharmaceutical research[3] to planetary sciences[4]. Among the many ways to address this need, considerable effort has been put in miniaturizing the most widespread Fourier Transform Spectroscopy (FTS) technique[5–7], which relies on interfering light with a delayed copy of itself to produce an autocorrelation signal as a function of optical delay, known as the interferogram. Whereas FTS has the distinct advantage of compatibility with any light source, including an incoherent thermal emitter, its resolution is inversely proportional to the maximum optical path difference (OPD)[8], which imposes a practical limit in the sub-THz range for compact spectrometers. One way to overcome this is to employ an optical frequency comb (OFC) with discrete spectral structure. OFCs also offer straightforward calibration of the spectral axis and extremely high brightness per spectral element[9].

While OFC sources can enable chip-scale FTS to surpass the OPD resolution limit[10], particular attention has been devoted in recent years to the rival technique of dual-comb spectroscopy (DCS)[11], which retrieves broadband and high-resolution spectral information from a fast photodetector through optical multi-heterodyne beating with a second comb[12] rather than itself. This approach relaxes the OPD-imposed resolution limit by enabling line-resolved spectroscopic assessments, although it naturally relies on the availability of a stable comb source and a high-speed optical detector operating in the relevant spectral region. Following early table-top demonstrations[13], the progress in miniaturization has recently resulted in extremely compact battery-operated OFC generators[14]. This has paved the way toward smart spectroscopic sensors operating in the technologically-mature near-infrared region. However, a large gap remains between these advances and the less-developed, but spectroscopically-more-relevant, mid- and far-infrared regions that contain the strongest molecular transitions[15].

Broadband molecular DCS within a self-contained platform has never been demonstrated to date. So-called self-detected DCS platforms have allowed multi-heterodyne beat notes to be observed in the terahertz range using a pair of cryogenic QCLs[16–18], and in the mid-infrared under microwave injection locking conditions[19]. However, these techniques that rely on illuminating one comb (LO – local oscillator) with another comb (signal) are limited by the optical injection locking effect. Hence, microwave injection is required to prevent the LO comb from following the signal due to injection locking. One can naturally reduce the coupling to the LO comb, but only at the expense of lower DCS signal-to-noise ratio (SNR). It would therefore be of great interest to have a single room-temperature device structure that operates as a mid-infrared frequency comb when biased above threshold, but also as a sensitive and fast photodetector (which uses multi-heterodyne beating to down-convert spectroscopic information from the optical to the electrical domain) when operated at zero or negative bias. This intriguing opportunity can in fact be realized using bi-functional quantum cascade[20] and interband cascade lasers (QCLs and ICLs)[21,22]. In particular, we expect monolithic DCS platforms based on ICL bi-functional devices[22,23] to play a key role in future on-chip spectrometers. Prior mid-infrared DCS experiments[24–29] have employed external, thermoelectrically-cooled photodiode detectors (usually $Hg_{1-x}Cd_xTe$ / MCT) that are incompatible with full on-chip integration.

In this work, we present mid-infrared molecular dual-comb spectroscopy measurements using room-temperature, free-running, low-power, electrically-pumped sources and detectors that are fabricated from the same material. By replacing a pair of MCT detectors with a single IC detector, we have substantially improved the system power budget and minimized its footprint, while maintaining intact the spectroscopic performance. Previously, the multi-stage thermoelectric cooling required for fast operation of MCT consumed a few watts of electrical power, whereas the driving electronics required active heat dissipation. The sub-millimeter sized IC detector is

[a)] Electronic mail: Mahmood.Bagheri@jpl.nasa.gov

free of these encumbrances – it requires at most a few milliwatts of electrical power with virtually no self-generated heat. Careful optical feedback management has also stabilized the sources sufficiently that ordinary video-averaging of the dual-comb spectra is permitted, without any phase post-correction routines[30] or advanced hardware feedback loops.

Both ICL frequency combs and interband cascade photodetectors (ICIPs) were processed from the same GaSb-based wafer material, which was designed and grown as discussed in Ref. 23,31. To characterize the performance of the ICIPs used in the broadband DCS reported below, we first cleaved a 400 μm long Fabry-Pérot device from the wafer and mounted it on a beryllium oxide submount with patterned gold contacts that provided a ground-signal-ground microwave probe. A black diamond lens with high numerical aperture focused light from an ICL comb emitting at $\lambda = 3.6$ μm onto the photodetector facet. The resulting DC electrical and spectral responsivities at room-temperature are plotted in Fig. 1. The current-voltage (I-V) characteristics depicted in Figs. 1a and Fig. 1b were collected under dark and illuminated conditions using a Keithley 2420 Source Meter. The photovoltaic performance highlighted by the shaded area, is delineated by the short circuit current (I_{sc}) and open-circuit voltage (V_{oc}), which are 33.5 μA and 0.267 V, respectively, when the device is illuminated by 3.8 mW of power from the ICL comb. That these values are 3–4 times lower than what was reported previously for an on-chip ICL laser-detector pair[21] is attributed to lower light coupling efficiency into the IC detector. The earlier experiment obtained 9% collection efficiency by coupling the light from a laser facet into a 12 μm wide ridge waveguide located just 12 μm away, whereas our beam was collimated and focused by external free-space optics into a waveguide that was 3 times narrower (3.5 μm). That naturally rendered the coupling less effective and lowered the responsivity. To estimate how much light is coupled into the photodetector's optically-active area under edge illumination, we first project the responsivity limited by the external quantum efficiency (EQE)[21]. Accounting for the ∼30% reflection loss at the uncoated air-detector interface, we obtain 10% EQE for our 7-stage devices. The corresponding room-temperature responsivity (R_λ) at 3.6 μm is 290 mA/W. Next, the power incident on the detector's active area is estimated from the short-circuit current through $P_i = I_{sc}/R_\lambda$, and compared with that available before the coupling lens. The coarse estimate that 115.5 μW of light is coupled corresponds to a coupling efficiency of ∼3.4%. Nevertheless, this level is more than sufficient for many spectroscopy applications.

To retrieve the zero-bias spectral responsivity (Fig. 1c), we illuminated the ICIP facet with a globar source from a Bruker Vertex 80 Fourier Transform Spectrometer, which was calibrated using an MCT photodetector with known responsivity characteristics. The ICIP photocurrent was amplified with an SRS810 lock-in transimpedance amplifier, whose voltage output was fed to the FTIR's external detector acquisition channel along with the optical chopper reference signal for the step-scan measurement. The measured relative responsivity spectrum was next normalized by the incident optical power at the laser wavelength[32]. The rapid responsivity roll-off at

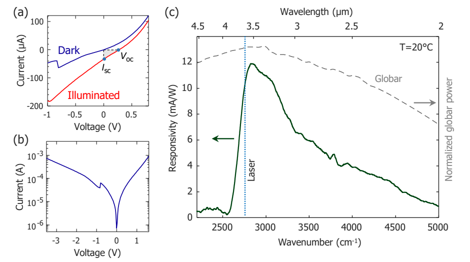

FIG. 1. Electrical and optical characteristics of the ICIP. (a) Linear and (b) log-scale plot of the dark and illuminated (linear curve only) I-V response. For an illumination power of 3.8 mW at 3.6 μm, the short-circuit current I_{sc} is 33.5 μA while the open-circuit voltage V_{oc} is 0.267 V. At room temperature the differential resistance at zero bias is 15 kΩ, which corresponds to ∼100 pW×Hz$^{-1/2}$ of Johnson-noise-limited noise-equivalent power (NEP). (c) Spectral responsivity of the ICIP for edge coupling (solid curve), under illumination by a globar source with normalized power given by the dashed curve. The vertical dotted line indicates the emission wavelength from the same material when it is operated under forward bias as a laser.

longer wavelengths approaches a 90% cutoff at 3.85 μm, only 250 nm longer than the laser wavelength. At shorter wavelengths, the responsivity slowly decays through about 2 μm. This decrease, which was also observed in Ref. 21, is due to an increase in parasitic absorption losses outside the active IC core at shorter wavelengths when the detector is illuminated from the edge. Nevertheless, the peak sensitivity at 3.5 μm reaches ∼12 mA/W at room temperature without any correction for reflection loss or coupling efficiency.

Having characterized the ICIP, we multi-heterodyned two unstabilized ICL combs (cleaved from the same wafer as the detector) in the dual-comb configuration shown schematically in Fig. 2a. A pair of Vescent Photonics D2-105-500 drivers controlled the laser currents and temperatures. The signal comb interrogated the $L = 5$ cm long gas absorption cell prior to being combined on a beam splitter with the repetition-rate-mismatched (Δf_{rep} = 23 MHz) local oscillator comb. The 4 mm long devices with ∼9.7 GHz repetition rates operated at temperatures of 20.7°C and 26.7°C, with injection currents of 300 mA and 234 mA for the local oscillator and signal combs, respectively. The electrical power delivered to each laser was < 1 W. Because the detector surface is highly reflective (∼30%), direct illumination generally causes optical feedback that induces instabilities in the comb operation. In this experiment, the insertion of a 30 dB optical isolator drastically improved the stability of the DCS system compared to our previous works[27,29] (discussed further below). This modification eliminated the need to normalize the power using a matched reference photodetector. We see from the spectra in Fig. 2b that the two combs developed 25–30-nm bandwidths centered around 3.62 μm. Their mutual overlap provides ∼600 GHz of optical coverage mapped to 1.4 GHz of radio frequency (RF) bandwidth. To calibrate the optical frequency axis in the RF signal, we relied on the knowledge of

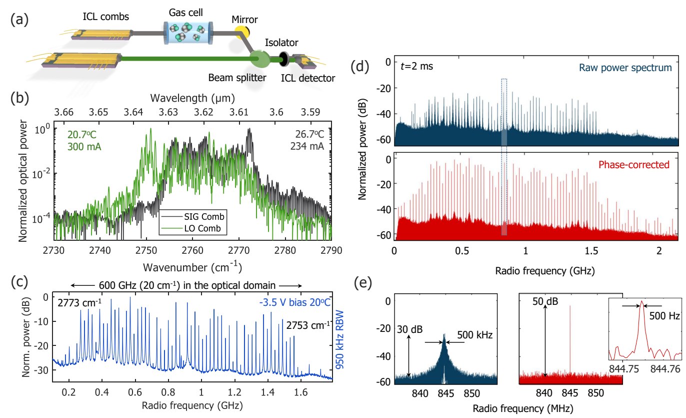

FIG. 2. Free-running dual-comb beating on the ICIP operating at room temperature. (a) Experimental setup. (b) Optical spectra measured with an FTIR of the two mid-IR ICL combs operating slightly above room temperature and consuming less than 1 W of electrical power each. (c) Free-running dual-comb beating spectrum obtained by averaging 500 short (4 μs) power spectra that were acquired within 2 ms without any computational phase manipulation. Such spectra were used for spectroscopy. (d) Characterization of the free-running linewidths and computational correction efficacy. The raw power spectrum (top) was obtained by Fourier-transforming the full 2 ms long dual-comb beating signal. The SNR is considerably improved with the CoCoA[30] phase correction algorithm (bottom panel), which cancels out multiplicative phase noise from the comb lines. (e) Despite the initial high signal-to-noise (up to 30 dB) and low free-running linewidth of the RF comb lines (∼500 kHz), further improvement of the DCS signal quality is possible. A phase-noiseless signal would gain 20 dB within 2 ms of acquisition.

the combs' repetition rates along with the FTIR-measured positions of the two characteristic LO comb lines at 2763.6 cm^{-1} and 2764.6 cm^{-1}.

In the multi-heterodyne experiment, we reverse-biased the room-temperature ICL detector to improve its electrical high-frequency response (see below), and used a 40 dB gain broadband amplifier to increase the microwave signal extracted from the RF port of a bias tee. The signal was next recorded for 2 ms with a Lecroy WavePro7Zi-A oscilloscope. Figure 2c plots the reverse-mapped dual-comb (multi-heterodyne) spectrum derived from optical beating between the two free-running combs, as detected with the ICIP. This plot was generated by ordinary (video) averaging five hundred 4-μs-long power spectra without any phase manipulation or post-correction. In contrast to our previous experiments without an optical isolator, the individual RF comb lines are easily resolved. This eliminates the need for sophisticated signal processing in the target sensing platform. Instead, the transmission can be estimated by ordinary averaging of the Fast Fourier Transform (FFT) squared magnitude spectra, known as the Welch's modified periodogram averaging method[33], albeit at the expense of signal-to-noise ratio and lost phase information due to the incoherent averaging. Figure 2d was generated from a conventional Fourier transform of the entire 2-ms-long dual-comb interferogram. This still possesses the discrete comb structure with 500 kHz RF beat note linewidth and 30 dB peak signal-to-noise ratio. The high relative power of the beat notes is comparable to those of dual-comb systems employing dedicated thermoelectrically-cooled photodetectors. From the RF beat note linewidth, we estimate a free-running optical comb linewidth of ∼350 kHz on a 2 ms time scale. This order-of-magnitude improvement over our initial demonstrations of ICL-based DCS[29] is attributable to the effective feedback management provided by the optical isolator.

Excessive phase noise in the laser signal can corrupt a DCS system's apparent RF signal-to-noise level. To estimate the quality of the DCS signal detected by our room-temperature photodiode in the absence of phase noise, we have self-corrected for phase and frequency noise using the CoCoA algorithm[30]. This extracts the instantaneous RF comb repetition rate $\Delta f_{\mathrm{rep}}(t)$ and offset frequency $\Delta f_0(t)$, and corrects for their non-stationarity. While the operation may at first look like a computational trick that renders RF linewidths limited by the acquisition time, it has provided spectroscopic validity in numerous dual-comb platforms[28]. The lower panel of Fig. 2d shows that following phase-correction (and resampling) of the spectrum, most of the RF lines have SNR exceeding 30 dB, while the strongest lines reach 50 dB. A side-by-side comparison of the same line at 845 MHz, shown in Fig. 2e, reveals 20 dB of correction gain and an acquisition-time-limited linewidth of ∼500 Hz. Moreover, the simultaneous narrowing and amplification of all the RF comb lines proves their high phase noise correlation. In principle, the appearance after the correction of weaker lines with 10–15 dB of SNR should allow extension of the spectral coverage to ∼840 GHz. However, since practical low-power spectrometers lack the high computational power needed for digital phase correction, we restricted the analysis to ordinary averaging of the Fourier power spectrum. This limited the usable optical coverage to ∼600 GHz.

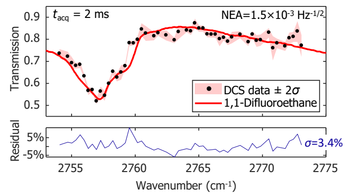

FIG. 3. Experimental (points) and simulated (curve) spectrum of 1,1-difluoroethane at atmospheric pressure. The standard deviation of the residual between the DCS data and HITRAN2016 model is 3.4%, corresponding to NEA of 1.5×10^{-3} $\mathrm{Hz}^{-1/2}$.

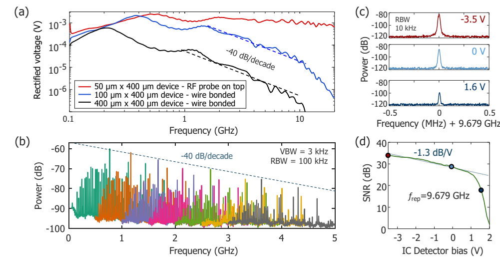

FIG. 4. (a) Microwave rectification[32] characterization of ICIP devices with three different lengths and two alternative electrical connection schemes. (b) Optical heterodyne characteristics of the 400×400 μm wire-bonded device acquired with a microwave spectrum analyzer. (c) Optically-detected intermode beat note at different reverse bias voltages. The source and detector were separated by more than 1 m to avoid any pickup of the microwave signal. (d) Free-running signal-to-noise ratio of the intermode beat note as a function of bias. The dashed line indicates that the response improves by approximately –1.3 dB/V at negative voltages.

As a molecular target we chose Freon-152a refrigerant (1,1-difluoroethane, DFE), a spectrally broadband organofluorine compound with the chemical formula CHF_2CH_3. It is envisioned as an alternative to the hydrofluorocarbon refrigerants commonly used in domestic and automotive air conditioners, because it does not deplete ozone. The absorption cell was filled with the gas at atmospheric pressure and room temperature, and a zero-gas reference was acquired. The DCS spectrum shown in Fig. 3 was then obtained with the ICIP, and processed using the Welch's averaging method. We used a flat top window in the calculation of the overlapped segments spectra, as it provides improved robustness against inaccurate peak detection often leading to large errors in comb teeth amplitude estimates. Furthermore, no baseline correction has been applied to the transmission spectrum – the data was obtained directly from the ratio of raw zero-gas reference to gas sample spectrum. The broad absorption feature at 2757 cm^{-1} is simulated using an absorption cross-section model based on the HITRAN2016 database[34]. We exclude RF beat notes weaker than –18 dB (relative), and calculate 2σ confidence intervals for the $M = 51$ remaining ones based on formulae in Ref. 26. The DCS-based transmission spectrum (points) agrees well with the model (curve), as reflected in the low standard deviation of the residual. We obtain $\sigma = 3.4\%$, which corresponds to a noise-equivalent absorption (NEA) of 1.5×10^{-3} $\mathrm{Hz}^{-1/2}$. This is comparable to the values obtained previously with ICL-based dual-comb spectrometers[27,29], which proves that the present setup's far greater simplicity and lower cost have not sacrificed performance.

From a chemical sensing perspective, of interest may be the system detection sensitivity. The minimum detectable absorption coefficient per spectral element α_{min}=NEA/(LM) is 5.9×10^{-6} $\mathrm{cm}^{-1}\cdot\mathrm{Hz}^{-1/2}$. This value allows to detect 1500 part-per-million by volume (ppmv) of DFE in a 5 cm absorption path at 1 s of integration. However, 1 s DFE detection limits of dozens of ppm are possible by targeting absorption bands located at 3.36 μm with >100× larger absorption cross-sections using future shorter-wavelength ICLs. Alternatively, if the setup compactness is not a requirement, enhancement of the 5 cm absorption path with a Herriott cell as in Ref. 29 should enable detection levels in a parts-per-billion (ppb) range.

Finally, to evaluate the effects of electrical parasitics on the ICIP response, we cleaved two additional devices with the same 400 μm top gold contact width but 4 and 8 times shorter in length (100 μm, and 50 μm). The electrical responses of these and the original device were characterized in a microwave rectification experiment[35] that injected a microwave (GHz) carrier signal with kHz-rate amplitude modulation into the detector through a bias tee, while the rectified voltage was measured by a lock-in amplifier. The frequency response characteristics plotted in Fig. 4a show two general regions: hundreds of MHz where the parasitic LC resonance dominates and GHz where low-pass roll-off occurs. We see that lowering the device's capacitance by ×4 shifts the parasitic resonance at sub-GHz frequencies by approximately a factor of two. This is accompanied by lower attenuation of the higher-frequency response, as well as a shift of the low-pass corner frequency. The 50 μm device has the flattest microwave response, owing to the lack of wire bonding since that device was measured with a microwave probe on top. This suggests that multi-GHz bandwidths may become possible with future optimization of the packaging and impedance matching[36]. To validate the agreement between the microwave rectification and optical heterodyne characteristics, the multi-heterodyne beating spectrum was measured for the longest detector (lasing at positive bias). Different injection currents (in steps of 2 mA above 250 mA) were supplied to the local oscillator, while the signal comb remained biased at a fixed value. Laser injection current simultaneously changes the ICL comb offset frequency f_0 and repetition rate f_{rep} via thermal tuning of the refractive index and thus allows to tune the comb's frequencies. Although f_{rep} varies by sub-MHz values across the scan, it induces spectral shifts approximately N times larger, where $N \approx 8560$ here is the order the comb's center line. Fig. 4b shows that the strongest peak in the dual-comb RF spectrum follows a roll-off curve of approximately –40 dB/decade. Thus from a practical standpoint, the

ICIP remains useful at frequencies close to half the repetition rate (4.5 GHz) with a SNR of 20 dB for the strongest lines, which enables future gapless DCS experiments[37] exploiting the wide electrical tunability of ICL combs. We also find that reverse-biasing the ICIP improves the frequency response even further, due to faster carrier extraction. Figs. 4c,d show that the SNR of the signal comb's optically-detected RF beat note at ∼9.7 GHz exceeds 30 dB at zero bias, and increases by –1.3 dB/V when a reverse bias is applied.

In conclusion, we have shown that mid-infrared type-II ICL frequency combs are perfect candidates for future monolithic, chip-scale, dual-comb spectroscopic platforms operating at room temperature with low power consumption. The bi-functional ICL/ICIP capability allowed us to implement a self-contained free-running DCS with performance, as characterized by the spectroscopic noise equivalent absorption and spectral coverage, comparable to more complex systems with commercial off-the-shelf MCT detectors. While the microwave response of our current ICIP is limited by electrical parasitics, those can be addressed straightforwardly through optimization of the detector size and packaging. Also the EQE can be improved in future designs to ∼20% by employing anti-reflection (AR) coated devices with a reduced number of stages (i.e. five) while maximizing the light coupling efficiency to the detector. And whereas the self-contained DCS platform demonstrated here is chip-based rather than on-chip, we envision truly monolithic broadband spectrometers[38] with plasmonic waveguides that enhance the sensitivity to ambient analytes[20]. Given the successful deployment of ICL-based spectrometers on Mars[39], the ICL comb's extension of single-mode lasing into > 100 phase locked modes will enable the implementation of solar-powered, tunable mid-infrared dual-comb spectrometers for terrestrial and space applications.

ACKNOWLEDGMENTS

This work was supported under National Aeronautics and Space Agency's (NASA) PICASSO program (106822 / 811073.02.24.01.85) and was in part performed at the Jet Propulsion Laboratory (JPL), California Institute of Technology, under contract with the NASA. L. A. Sterczewski's research was supported by an appointment to the NASA Postdoctoral Program at JPL, administered by Universities Space Research Association under contract with NASA. The NRL authors acknowledge support from the Office of Naval Research (ONR);

REFERENCES

[1] R. N. Clark and T. L. Roush, Journal of Geophysical Research: Solid Earth **89**, 6329–6340 (1984).
[2] R. Boushel and C. Piantadosi, Acta Physiologica Scandinavica **168**, 615–622 (2000).
[3] J. Luypaert, D. Massart, and Y. Vander Heyden, Talanta **72**, 865–883 (2007).
[4] R. N. Bracewell and R. H. MacPhie, Icarus **38**, 136–147 (1979).
[5] M. Nedeljkovic, A. V. Velasco, A. Z. Khokhar, A. Delâge, P. Cheben, and G. Z. Mashanovich, IEEE Photonics Technology Letters **28**, 528 (2016).
[6] M. C. Souza, A. Grieco, N. C. Frateschi, and Y. Fainman, Nature communications **9**, 665 (2018).
[7] D. Pohl, M. R. Escalé, M. Madi, F. Kaufmann, P. Brotzer, A. Sergeyev, B. Guldimann, P. Giaccari, E. Alberti, U. Meier, *et al.*, Nature Photonics **14**, 24–29 (2019).
[8] R. Bell, *Introductory Fourier transform spectroscopy* (Elsevier, 2012).
[9] S. A. Diddams, JOSA B **27**, B51–B62 (2010).
[10] P. Maslowski, K. F. Lee, A. C. Johansson, A. Khodabakhsh, G. Kowzan, L. Rutkowski, A. A. Mills, C. Mohr, J. Jiang, M. E. Fermann, *et al.*, Physical Review A **93**, 021802 (2016).
[11] I. Coddington, N. Newbury, and W. Swann, Optica **3**, 414–426 (2016).
[12] D. van der Weide and F. Keilmann, *Coherent periodically pulsed radiation spectrometer* (Google Patents, 1998).
[13] F. Keilmann, C. Gohle, and R. Holzwarth, Optics Letters **29**, 1542 (2004).
[14] B. Stern, X. Ji, Y. Okawachi, A. L. Gaeta, and M. Lipson, Nature **562**, 401 (2018).
[15] G. Scalari, J. Faist, and N. Picqué, Applied Physics Letters **114**, 150401 (2019).
[16] M. Rösch, G. Scalari, G. Villares, L. Bosco, M. Beck, and J. Faist, Applied Physics Letters **108**, 171104 (2016).
[17] M. Rösch, M. Beck, M. J. Süess, D. Bachmann, K. Unterrainer, J. Faist, and G. Scalari, Nanophotonics **7**, 237 (2018).
[18] H. Li, Z. Li, W. Wan, K. Zhou, X. Liao, S. Yang, C. Wang, J. C. Cao, and H. Zeng, ACS Photonics **7**, 49 (2020).
[19] J. Hillbrand, A. M. Andrews, H. Detz, G. Strasser, and B. Schwarz, Nature Photonics **13**, 101 (2019).
[20] B. Schwarz, P. Reininger, D. Ristanić, H. Detz, A. M. Andrews, W. Schrenk, and G. Strasser, Nature Communications **5**, 1 (2014).
[21] H. Lotfi, L. Li, S. M. Shazzad Rassel, R. Q. Yang, C. J. Corrége, M. B. Johnson, P. R. Larson, and J. A. Gupta, Applied Physics Letters **109**, 151111 (2016).
[22] B. Schwarz, J. Hillbrand, M. Beiser, A. M. Andrews, G. Strasser, H. Detz, A. Schade, R. Weih, and S. Höfling, Optica **6**, 890 (2019).
[23] M. Bagheri, C. Frez, L. A. Sterczewski, I. Gruidin, M. Fradet, I. Vurgaftman, C. L. Canedy, W. W. Bewley, C. D. Merritt, C. S. Kim, M. Kim, and J. R. Meyer, Scientific Reports **8**, 3322 (2018).
[24] G. Villares, A. Hugi, S. Blaser, and J. Faist, Nature communications **5**, 5192 (2014).
[25] G. Ycas, F. R. Giorgetta, E. Baumann, I. Coddington, D. Herman, S. A. Diddams, and N. R. Newbury, Nature Photonics **12**, 202 (2018).
[26] J. Westberg, L. Sterczewski, and G. Wysocki, Applied Physics Letters **110**, 141108 (2017).
[27] L. A. Sterczewski, J. Westberg, C. L. Patrick, C. S. Kim, M. Kim, C. L. Canedy, W. W. Bewley, C. D. Merritt, I. Vurgaftman, J. R. Meyer, *et al.*, Optical Engineering **57**, 011014 (2017).
[28] J. Westberg, L. A. Sterczewski, F. Kapsalidis, Y. Bidaux, J. M. Wolf, M. Beck, J. Faist, and G. Wysocki, Optics Letters **43**, 4522–4525 (2018).
[29] L. A. Sterczewski, J. Westberg, M. Bagheri, C. Frez, I. Vurgaftman, C. L. Canedy, W. W. Bewley, C. D. Merritt, C. S. Kim, M. Kim, J. R. Meyer, and G. Wysocki, Optics Letters **44**, 2113 (2019).
[30] L. A. Sterczewski, J. Westberg, and G. Wysocki, Optics Express **27**, 23875 (2019).
[31] C. L. Canedy, J. Abell, C. D. Merritt, W. W. Bewley, C. S. Kim, M. Kim, I. Vurgaftman, and J. R. Meyer, Optics Express **22**, 7702 (2014).
[32] Y. Zhou, S. Zhai, F. Wang, J. Liu, F. Liu, S. Liu, J. Zhang, N. Zhuo, L. Wang, and Z. Wang, AIP Advances **6**, 035305 (2016).
[33] P. Welch, IEEE Transactions on audio and electroacoustics **15**, 70–73 (1967).
[34] R. V. Kochanov, I. E. Gordon, L. S. Rothman, K. P. Shine, S. W. Sharpe, T. J. Johnson, T. J. Wallington, J. J. Harrison, P. F. Bernath, M. Birk, G. Wagner, K. Le Bris, I. Bravo, and C. Hill, Journal of Quantitative Spectroscopy and Radiative Transfer **230**, 172 (2019).
[35] H. C. Liu, Buchanan, M., and Z. R. Wasilewski, IEEE Journal of Quantum Electronics **32**, 1024 (1996).
[36] Y. Chen, X. Chai, Z. Xie, Z. Deng, N. Zhang, Y. Zhou, Z. Xu, J. Chen, and B. Chen, Journal of Lightwave Technology **38** (2019).
[37] M. Gianella, A. Nataraj, B. Tuzson, P. Jouy, F. Kapsalidis, M. Beck, M. Mangold, A. Hugi, J. Faist, and L. Emmenegger, Optics Express (2020), 10.1364/OE.379790.
[38] J. R. Meyer, I. Vurgaftman, C. L. Canedy, W. W. Bewley, C. S. Kim, C. D. Merritt, R. J. Warren, R. J. Weiblen, and M. Kim, "Highly stable semiconductor lasers and sensors for III-V and silicon photonic integrated circuits," (2019).
[39] C. R. Webster, P. R. Mahaffy, S. K. Atreya, G. J. Flesch, M. A. Mischna, P.-Y. Meslin, K. A. Farley, P. G. Conrad, L. E. Christensen, A. A. Pavlov, *et al.*, Science **347**, 415–417 (2015).

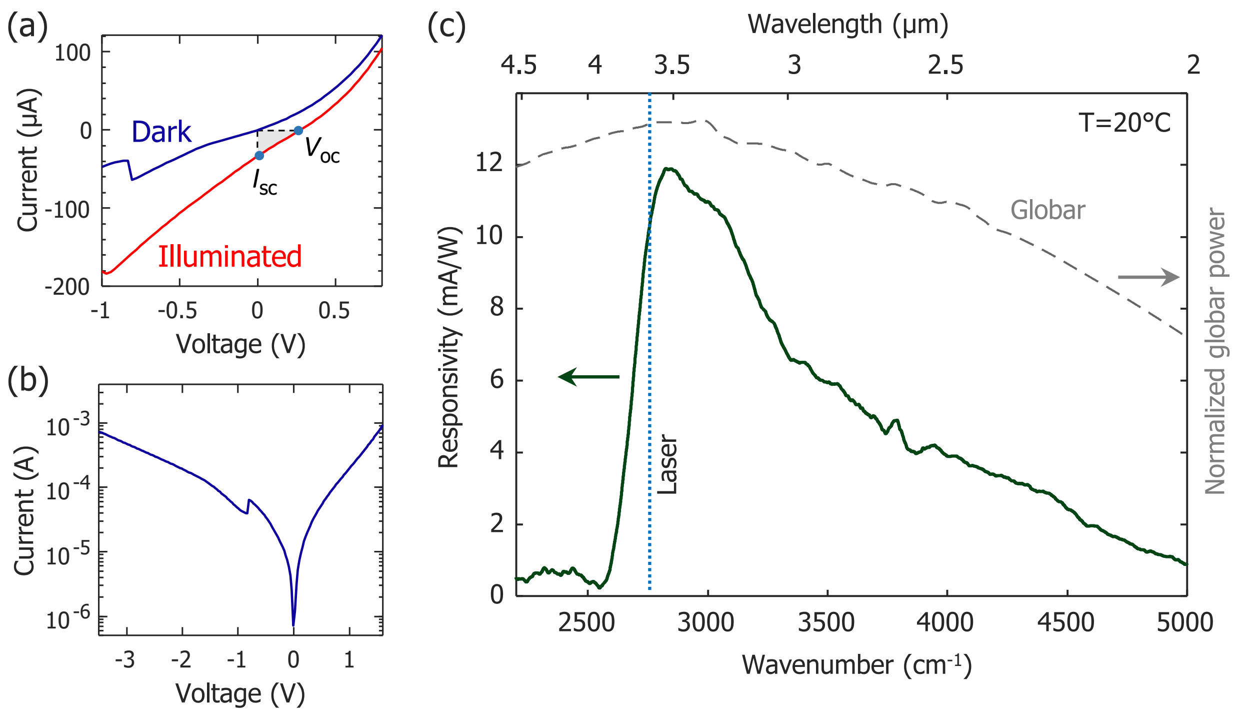
(a)
Current (μA)
Voltage (V)
Dark
Illuminated
V_{oc}
I_{sc}
(b)
Current (A)
Voltage (V)
(c)
Wavelength (μm)
T=20°C
Globar
Laser
Responsivity (mA/W)
Normalized globar power
Wavenumber (cm-1)

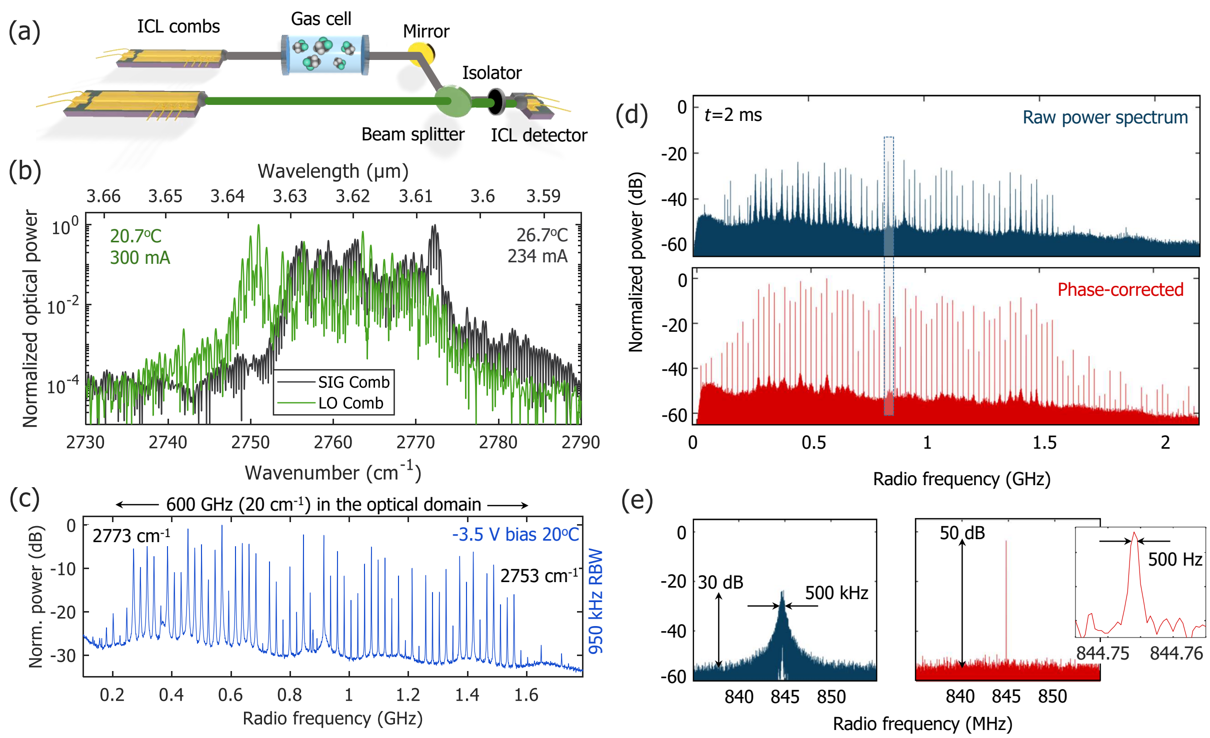
(a)
ICL combs
Gas cell
Mirror
Isolator
Beam splitter
ICL detector
(b)
Wavelength (μm)
3.66
3.65
3.64
3.63
3.62
3.61
3.6
3.59
20.7°C
300 mA
26.7°C
234 mA
Normalized optical power
10^0
10^{-2}
10^{-4}
SIG Comb
LO Comb
2730
2740
2750
2760
2770
2780
2790
Wavenumber (cm^{-1})
(c)
600 GHz (20 cm^{-1}) in the optical domain
2773 cm^{-1}
-3.5 V bias 20°C
2753 cm^{-1}
950 kHz RBW
Norm. power (dB)
0
-10
-20
-30
0.2
0.4
0.6
0.8
1
1.2
1.4
1.6
Radio frequency (GHz)
(d)
t=2 ms
Raw power spectrum
Phase-corrected
Normalized power (dB)
0
-20
-40
-60
0
0.5
1
1.5
2
Radio frequency (GHz)
(e)
30 dB
500 kHz
50 dB
500 Hz
844.75
844.76
0
-20
-40
-60
840
845
850
Radio frequency (MHz)

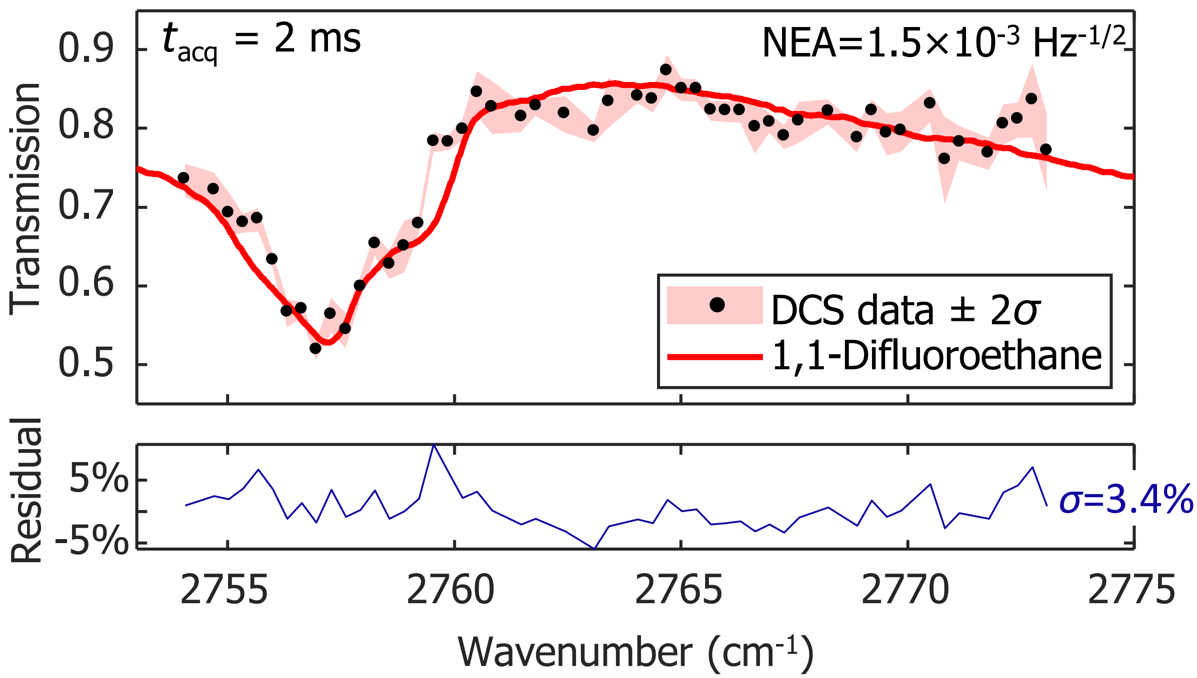
t_{acq} = 2 ms
NEA=1.5×10^{-3} Hz$^{-1/2}$
Transmission
0.9
0.8
0.7
0.6
0.5
DCS data ± 2σ
1,1-Difluoroethane
Residual
5%
-5%
σ=3.4%
2755
2760
2765
2770
2775
Wavenumber (cm^{-1})

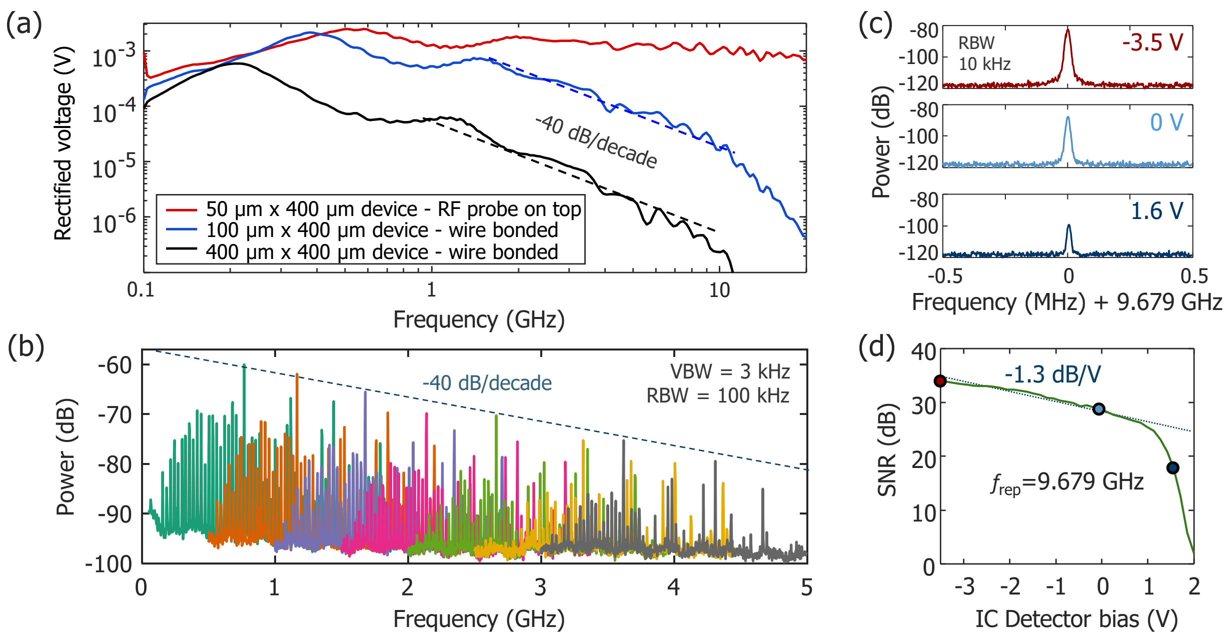
(a)
Rectified voltage (V)
-40 dB/decade
50 µm x 400 µm device - RF probe on top
100 µm x 400 µm device - wire bonded
400 µm x 400 µm device - wire bonded
Frequency (GHz)
(b)
Power (dB)
-40 dB/decade
VBW = 3 kHz
RBW = 100 kHz
Frequency (GHz)
(c)
RBW
10 kHz
-3.5 V
0 V
1.6 V
Power (dB)
Frequency (MHz) + 9.679 GHz
(d)
-1.3 dB/V
SNR (dB)
f_{rep}=9.679 GHz
IC Detector bias (V)